WILEY | Hindawi

Research Article

Two-Stage Optimization Model of Centralized Energy Storage Participating in Peak Shaving with Maximum Reserve Capacity and Minimum Carbon Emission of the System

Zhiyao Zhang [iD],[1] **Jingjie Huang** [iD],[1] **Nianguang Zhou** [iD],[2] **Hongming Yang** [iD],[1] **and Renjun Zhou** [iD][1]

[1]*Hunan Province Collaborative Innovation Center of Clean Energy and Smart Grid,*
 Changsha University of Science and Technology, Changsha 410004, China
[2]*Research Institute of Economics and Technology of State Grid Hunan Electric Power Co., Ltd., Changsha 410004, China*

Correspondence should be addressed to Jingjie Huang; jingjie.huang@outlook.com and Renjun Zhou; zrj0731@csust.edu.cn

As the proportion of renewable energy increases in power systems, the need for peak shaving is increasing. The optimal operation of the battery energy storage system (BESS) can provide a resilient and low-carbon peak-shaving approach for the system. Therefore, a two-stage optimization model for grid-side BESS is proposed. First, the carbon emission model of thermal power units considering BESS is proposed to describe the ability of the BESS in reducing the carbon emissions. Second, in order to deal with the uncertainty of the photovoltaics and wind forecast errors, a certain capacity of BESS is reserved. The model in the first stage takes the lowest carbon emission of the system as the goal, and the model in the second stage determines the BESS reserve capacity with the objective of minimizing the risk cost of the system. The simulation results show that the carbon emission model of thermal power units with BESS can measure the contribution of energy storage to emission reduction. By setting the reserve capacity of energy storage, the peak-shaving resilience of the system is improved, and the risk of photovoltaics and wind forecast error is reduced.

1. Introduction

As the installed capacity of wind power continues to increase, flexible adjustment resources are required to maintain safe and stable operation and power balance in the power system [1]. The requirements of peak shaving continue to increase due to the randomness and volatility of wind and solar power [2]. Coal-fired power plants are the most popular resource for the peak-shaving service. However, thermal power unit flexibility transformation for peak-shaving services is very expensive [3]. Besides, participating in peak shaving through the operation of thermal power units will increase its coal consumption, operation and maintenance costs, and carbon emissions, which is inconsistent with a national goal of peak carbon emissions by 2030 and carbon neutrality by 2060 in China [3]. The corresponding speed of peak shaving by hydropower units is

fast, but there is not enough hydropower for peak shaving in many areas due to the limitations of water resources and geography [4]. The peak-shaving capacity of hydropower is also limited by season, inflow, reservoir regulation capacity, etc. Therefore, in order to achieve low-carbon and flexible peak shaving, new devices and operation strategy are required.

The growth of renewable energy and the need for peak shaving have led to an exponential growth of grid support and storage installations around the globe. Consequently, by 2040 (accounting for 9 GW/17 GWh deployed as of 2018), the market will rise to 1095 GW/2,850 GWh, making a more than 120 times increase, based on a recent study published by Bloomberg New Energy Finance (BNEF) [5]. The fast and convenient control, simple requirements for geographical conditions, and high energy efficiency of energy storage devices can meet the need for a balance between supply and

demand [6, 7]. Most existing studies on energy storage analyze the economy of operation. For example, Hou et al. [8] developed a coupling operation model to optimize different energy storage devices for wind output power fluctuation smoothing, power imbalances mitigating, and peak load shaving with the maximum net earnings of the whole system. Authors in [9] proposed a resilient and peak-shaving trade-off scheme for battery energy storage systems to reduce operational costs. Authors in [10] developed a complex control algorithm in order to optimize the use of energy storage devices for peak load shaving in five different load demand profiles. Although reducing the operational costs of battery energy storage is of great importance, sometimes the revenue of energy storage should give way to the interests of renewable energy or power users, such as the centralized battery energy storage system (BESS) on the grid side [5].

BESS can be used for stationary applications at every level of the network such as generation, transmission, and distribution as well as local industrial and commercial customers [5]. At present, many countries and regions have successively built grid-side BESS. In the United States, Australia, and the Republic of Korea, grid-side BESS is mainly used to participate in the frequency modulation market and peak saving [11, 12]. There are also many grid-side BESS projects in China. For example, the grid-side distributed BESS project in Henan Province provides instruction tracking and output fluctuations smoothening services for the local power grid [13]. Zhicheng energy storage station, the first grid-side lead-carbon BESS in China, is mainly used in two typical application scenarios, namely, peak shaving and frequency regulation [14]. The Langli BESS in Hunan province [15] adopts the operation mode of "twice charging and twice discharging" in one day to meet the peak-shaving demand of load peak at noon and in the evening in that the load peak-valley difference is relatively large.

The research on centralized grid-side BESS is mainly about the economy of planning and operation. Authors in [16] developed a bi-level optimal locating and sizing model for a grid-side BESS, and the direct revenue of this system is from the arbitrage of the peak-valley electricity price and auxiliary service compensation. Authors in [6] proposed a probabilistic approach for sizing large-scale battery storage with the aim of mitigating the net load uncertainty and quantified the required BESS capacity for operating the wind plant without incurring excessive battery installation costs. A two-stage scheduling optimization model and solution algorithm for BESS with wind power considering uncertainty and demand response were proposed in [17]. For two-stage stochastic optimization models, the optimal sizing and location of BESS considering wind power integration were determined in [18]. Wind forecast errors will affect the operation of energy storage [19]. The existing research has not paid attention to the optimal operation of grid-side BESS, considering both the resilience issue of wind power and system carbon emissions in peak-shaving function [9, 20].

The measurement of the carbon emission reduction contribution of a certain device is conducive to the operation of the carbon market and carbon trading. In order to describe the carbon emission reduction contribution of grid-side BESS, the carbon emission measurement of the system needs a more accurate description first.

Therefore, in this paper, grid-side BESS is regarded as an independent centralized storage system, and its charge and discharge power are described and included in the carbon emission measurement of thermal power units. The value of system carbon emission intensity reduced by energy storage is related to the carbon emission intensity of thermal power units. Moreover, if a certain reserve capacity is set during the operation of energy storage, the system operation risk caused by the uncertain resilience issue of wind power and photovoltaics can be reduced, and the resilience of the system can be increased. When the economy of energy storage is reduced, the reserve capacity of the energy storage system will be increased, and the operation economy of the whole power system can be improved.

2. Carbon Emission Model of Thermal Power Units with BESS

China's coal-based energy structure determines that coal accounts for more than half of the primary energy. Therefore, this paper sets thermal power units as coal-fired thermal power units to simplify the description of the carbon emissions of thermal power units. According to the law of energy conservation, in an ideal situation, 122.8 g of standard coal is consumed to produce 1 kWh of electric energy. However, in fact, the coal consumption is far greater than 122.8 g/(kWh), and there are additional carbon emissions. In order to quantify the contribution of BESS to emission reduction in the system, it is first necessary to accurately describe the carbon emissions of thermal power units.

The carbon emission intensity or rate of coal-fired thermal power units is the amount of carbon dioxide emissions generated by 1 kWh of electricity supply for a unit and is negatively related to the power load. The higher the power load, the lower the carbon emission intensity [21]. Through linear fitting, the linear function relationship between the output of thermal power units and the carbon emission intensity is as follows [21]:

$$I_g\left(P_G^g(t)\right) = -k \cdot \left(\frac{P_G^g(t)}{P_{Gg}}\right) + b, \tag{1}$$

where $I_g\left(P_G^g(t)\right)$ is the carbon emission intensity of the unit g at hourly time interval t, $k \geq 0, b \geq 0$ are linear coefficients, $P_G^g(t)$ is the output of the unit g at time interval t, and P_{Gg} is the installed capacity of the unit g.

Then, the carbon emissions of the thermal power unit g can be calculated according to the following formula:

$$E_g\left(P_G^g(t)\right) = I_g \cdot P_G^g(t) \cdot \Delta t, \tag{2}$$

where Δt is the time between two consecutive time steps, in this paper, $\Delta t = 1$.

There is power loss from energy storage in the process of charging and discharging, which will cause additional carbon emissions. Therefore, when the renewable energy and

thermal power units can meet the load demand, the carbon emissions of the system are the lowest because the energy storage is not required to participate in peak shaving and there are no additional carbon emissions.

However, due to the forecast error of the power load and wind power and the limitation of the ramping power of thermal power units, it is necessary for BESS to meet the power balance needs and reduce the operation of thermal power units.

The BESS can also increase the output of low-coal consumption units and reduce the output of high-coal consumption units through reasonable charging and discharging. For example, low-coal consumption units can generate more electricity to provide energy storage, and when load increases, energy storage is first used instead of increasing the power of high coal consumption units.

Through storing excess wind power and discharging to reduce the output of thermal power units when wind power is insufficient, the BESS can reduce the carbon emissions of the system. The carbon emission model of thermal power units with BESS can be obtained as follows:

$$E_c\left(P_G^g(t), P_c^b(t), P_d^b(t)\right) = \sum_{t=1}^{T}\sum_{g=1}^{N_G} E_g\left(P_G^g(t)\right) - \omega_t \sum_{t=1}^{T}\sum_{b=1}^{N_B}\left(\left|P_c^b(t)\right| + \left|P_d^b(t)\right|\right), \tag{3}$$

where T is time intervals in one day, N_G is the number of thermal power units, ω_t is called the carbon emission intensity of BESS which is defined as carbon emission reduced by 1 kWh of charging or discharging, ω_t is related to the carbon emission intensity of thermal power units, N_B is the number of BESS, and $P_c^b(t)$ and $P_d^b(t)$ are charge and discharge power of the energy storage system b at time interval t.

The charging and discharging power changes the output of the thermal power units, resulting in changes in the carbon emission intensity of the thermal power units, thus changing the carbon emission of the system.

2.1. Upper Limit of ω_t.
Since there is power loss in the process of charging and discharging, the carbon emissions reduced by the BESS in formula (3) shall be less than the carbon emission of thermal power units. Therefore, the carbon emission intensity of BESS in formula (3) shall be less than the carbon emission intensity of thermal power units. And it can be ensured that wind power and photovoltaics instead of thermal power are used for energy storage charging. If the charging power is from thermal power units, the first term and the second term in formula (3) will increase at the same time, and the coefficient of the first term is greater than the second term, resulting in the increase of E_c.

$$\omega_t \le \min\left(I_1\left(P_G^1(t)\right), \ldots, I_g\left(P_G^g(t)\right), \ldots, I_{N_G}\left(P_G^{N_G}(t)\right)\right). \tag{4}$$

2.2. Lower Limit of ω_t.
The carbon emission of the system will not increase during the charging and discharging of energy storage. The value of ω_t should be greater than 0.

$$\omega_t \ge 0. \tag{5}$$

3. Risk-Cost Function with BESS

3.1. Risk-Cost Function of Wind Forecast Error with Reserve Capacity of BESS.
Due to the randomness and fluctuation of wind power and photovoltaics, the operation of thermal power units and BESS is needed to maintain the balance between power generation and power consumption. In this paper, the wind forecast error is mainly considered. The reserve capacity of flexible adjustment resources determines the allowable wind forecast error range. When the wind power exceeds the maximum allowable range, it will bring operational risks to the system and cause economic losses.

The probability density function $p\left(\Delta P_W^w(t)\right)$ of the wind or photovoltaics forecast error $\Delta P_W^w(t)$ of wind farm w can be modeled as a Gaussian distribution [22, 23]. As shown in Figure 1, $P_{W+}^w(t)$ and $P_{W-}^w(t)$, respectively, represent the upper and lower limits of the wind forecast error at time interval t. The upper and lower adjustable capacity of thermal power units and BESS can be determined as $[0, P_{W+}^w(t)]$ and $[P_{W-}^w(t), 0]$. When the wind forecast error at time t is less than $P_{W-}^w(t)$, the adjustable resources are insufficient and part of the load needs to be cut off. When the wind forecast error at time interval t is higher than $P_{W+}^w(t)$, measures such as wind abandonment shall be taken. Therefore, the probability-weighted average of the shaded part in Figure 1 can be used to represent the risk of load shedding and wind abandonment caused by wind forecast error at time interval t.

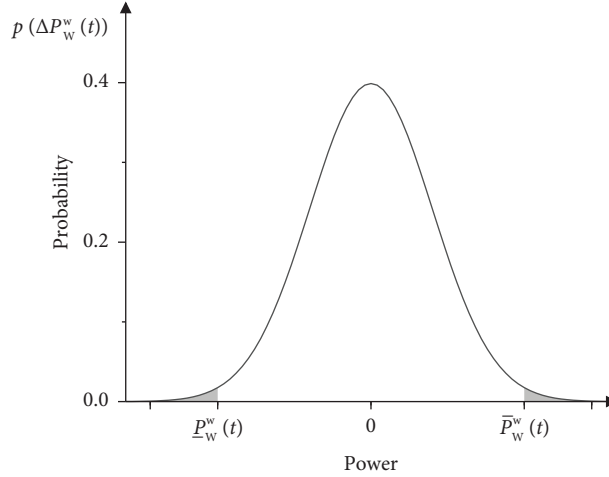Then, the risk-cost of wind abandonment and load shedding can be expressed as follows:

FIGURE 1: Probabilistic distribution of wind forecast error.

$$C_w = \sum_{t=1}^{T} \sum_{w=1}^{N_W} \left(\mu_W \int_{P_{W+}^w(t)}^{P_{Wmax}^w - P_W^w(t)} g(\Delta P_W^w(t)) d\Delta P_W^w(t) + \mu_L \int_{P_W^w(t) - P_{Wmin}^w}^{P_{W-}^w(t)} g(\Delta P_W^w(t)) d\Delta P_W^w(t) \right),$$

$$g(\Delta P_W^w(t)) = \Delta P_W^w(t) p(\Delta P_W^w(t)),$$

(6)

where N_W is the number of wind farms, P_{Wmax}^w and P_{Wmin}^w are the maximum and minimum power of wind farm w, μ_W and μ_L are penalty coefficients of wind abandonment and load shedding, and $P_W^w(t)$ is the power of wind farm w at time interval t.

Adding BESS to the system increases the system's adjustable capacity and can reduce the risk of wind abandonment and load shedding [24, 25]. The state of charge (SOC) of the BESS is maintained within an expected range to cope with the possible wind forecast error [26]. The risk cost function with reserve capacity of BESS is as follows:

$$C_{wb}(V_c^b(t), V_d^b(t)) = \sum_{t=1}^{T} \sum_{w=1}^{N_W} \sum_{b=1}^{N_B} \left(\mu_W \int_{P_{W+}^w(t)+V_c^b(t)}^{P_{Wmax}^w - P_W^w(t)} g(\Delta P_W^w(t)) d\Delta P_W^w(t) + \mu_D \int_{P_W^w(t) - P_{Wmin}^w}^{P_{W-}^w(t) - V_d^b(t)} g(\Delta P_W^w(t)) d\Delta P_W^w(t) \right),$$

(7)

where $V_c^b(t)$ and $V_d^b(t)$ are charging and discharging reserve capacity of BESS b at time interval t.

3.2. Operation Cost of Thermal Power Units. The power imbalance caused by the wind forecast error often requires the power of thermal power units to adjust, which will produce a certain fuel cost and operation cost, that is, the operation cost of thermal power units.

$$C_o(\Delta P_{Gu}^g(t), \Delta P_{Gd}^g(t)) = \sum_{t=1}^{T} \sum_{g=1}^{N_G} \left(\int_0^{\Delta P_{Gumax}^g(t)} y_u(\Delta P_{Gu}^g(t)) p(\Delta P_{Gu}^g(t)) d\Delta P_{Gu}^g(t) + \int_0^{\Delta P_{Gdmax}^g(t)} y_d(\Delta P_{Gu}^g(t)) p(\Delta P_{Gd}^g(t)) d\Delta P_{Gd}^g(t) \right),$$

$$y_u(\Delta P_{Gu}^g(t)) = C_g(P_G^g(t) + \Delta P_{Gu}^g(t)) - C_g(P_G^g(t)) + d_g|\Delta P_{Gu}^g(t)|,$$

$$d_d(\Delta P_{Gd}^g(t)) = C_g(P_G^g(t) - \Delta P_{Gd}^g(t)) - C_g(P_G^g(t)) + d_g|\Delta P_{Gd}^g(t)|,$$

$$C_g(P_G^g(t)) = a_g(P_G^g(t))^2 + b_g P_G^g(t) + c_g,$$

(8)

where $\Delta P_{Gumax}^g(t)$, $\Delta P_{Gdmax}^g(t)$, $\Delta P_{Gu}^g(t)$, and $\Delta P_{Gd}^g(t)$ are the maximum ramp up limit, the maximum ramp down limit, the ramp up power, and the ramp down power of the thermal power unit g at time interval t. C_g is

the fuel cost function of thermal power unit g, a_g, b_g, and c_g are fuel cost coefficients of thermal power unit g, d_g is the ramping cost coefficient of thermal power unit g.

4. Two-Stage Optimization Model of Grid-Side BESS with Maximum Reserve Capacity and Minimum Carbon Emission

4.1. Objective Function

4.1.1. Objective Function in the First Stage

$$\min F_1\left(P_G^g(t), P_c^b(t), P_d^b(t)\right) = k_1\rho + k_2 C_B + k_3 E_c, \qquad (9)$$

where k_1, k_2, and k_3 are weight coefficients and ρ, C_B, and E_c are the load peak-valley ratio, BESS operation cost function, and carbon emission function of thermal power units.

The equivalent load of the system is the sum of load power and BESS charging and discharging power.

$$P_{el}(t) = \sum_{k=1}^{N_K}\left(P_K^k(t)\right) + \sum_{b=1}^{N_B}\left(P_c^b(t) - P_d^b(t)\right), \qquad (10)$$

where N_K is number of nodes and $P_K^k(t)$ is the load power on node k at time t.

Then, the load peak-valley ratio of the equivalent load is as follows:

$$\rho = \frac{\max\left(P_{el}(t)\right) - \min\left(P_{el}(t)\right)}{\max\left(P_{el}(t)\right)} \times 100\%. \qquad (11)$$

The operation cost of BESS is as follows:

$$C_B = \sum_{i=1}^{N_B} c_{B,b}\left(\left|P_c^b(t)\right| + \left|P_d^b(t)\right|\right), \qquad (12)$$

where $c_{B,b}$ is the operation cost coefficient of BESS b.

4.1.2. Objective Function in the Second Stage.
The capacity of adjustable resources of the system is optimized in the second stage. The reserve capacity of BESS and the ramping power of thermal power units are adjusted to minimize risk cost function with BESS, including the risk cost of wind power and operation cost of thermal power units.

$$\min F_2\left(V_c^b(t), V_d^b(t), \Delta P_{Gu}^g(t), \Delta P_{Gd}^g(t)\right) = C_{wb}\left(V_c^b(t), V_d^b(t)\right) + C_o\left(\Delta P_{Gu}^g(t), \Delta P_{Gd}^g(t)\right). \qquad (13)$$

4.2. Constraints

4.2.1. Constraints in the First Stage

(a) Power balance constraint is as follows:

$$\sum_{w=1}^{N_W} P_W^w(t) + \sum_{g=1}^{N_G} P_G^g(t) + \sum_{b=1}^{N_B} P_d^b(t) = \sum_{k=1}^{N_L} P_K^k(t) + \sum_{i=1}^{N_B} P_c^b(t). \qquad (14)$$

(b) Wind power constraint is as follows:

$$P_{Wmin}^w \leq P_W^w(t) \leq P_{Wmax}^w. \qquad (15)$$

(c) Thermal power constraint is as follows:

$$P_{G,min}^g \leq P_G^g(t) \leq P_{Gmax}^g, \qquad (16)$$

where $P_{G,min}^g$ and $P_{G,max}^g$ are minimum and maximum power of thermal unit g.

(d) Ramping constraint of thermal power units is as follows:

$$r_d^g P_{Gmax}^g \leq P_G^g(t) - P_G^g(t-1) \leq r_u^g P_{Gmax}^g. \qquad (17)$$

(e) Start-stop constraints of thermal power units are as follows:

$$\begin{cases} \sum_{j=t}^{t+T_{g,on}-1} u_g(j) \geq T_{g,on}\left[u_g(t) - u_g(t-1)\right], \\ \sum_{j=t}^{t+T_{g,off}-1} \left(1 - u_g(j)\right) \geq T_{g,off}\left[u_g(t-1) - u_g(t)\right], \end{cases} \qquad (18)$$

where $u_g(j)$ represents the startup and shutdown status of the thermal unit g at time j, $u_g(j) = 0$ represents shutdown and $u_g(j) = 1$ represents startup, and $T_{g,on}$ and $T_{g,off}$ are the maximum continuous start and maximum continuous stop time of thermal unit g.

(f) BESS charge and discharge power constraints are as follows:

$$\begin{cases} 0 \leq P_c^b(t) \leq P_{cmax}^b, \\ 0 \leq P_d^b(t) \leq P_{dmax}^b, \end{cases} \qquad (19)$$

where $P_{c\,max}^b$ and $P_{d\,max}^b$ are maximum charge and discharge power of BESS b.

(g) State of charge constraints are as follows:

$$\begin{cases} S_b(t+1) = (1 - \sigma_b)S_b(t) - \dfrac{1}{V_{b,max}}\left(\eta_c^b P_c^b(t) - \dfrac{P_d^b(t)}{\eta_d^b}\right)\Delta t, \\ S_{b,min} \leq S_b(t) \leq S_{b,max}, \end{cases} \qquad (20)$$

where $S_b(t)$ is state of charge of BESS b at time interval t, $S_{b,max}$ and $S_{b,min}$ are upper and lower limits of state of charge, σ_b is the self-discharge rate, and η_c^b and η_d^b are the charge and discharge efficiency.

4.2.2. Constraints in the Second Stage.
After satisfying the constraints in the first stage, the variables to be solved in the second stage shall meet the following constraints:

(a) Adjustable power constraints of thermal power: The maximum adjustable power of the thermal power unit g at time interval t shall not exceed its

maximum ramping power, and thermal power shall not exceed its maximum and minimum power limits.

$$\begin{cases} 0 \leq \Delta P_{\mathrm{Gu}}^{g}(t) \leq \Delta P_{\mathrm{Gumax}}^{g}(t) \leq \min\left[(P_{\mathrm{Gmax}}^{g} - P_{G}^{g}(t)), r_{u}^{g}P_{\mathrm{Gmax}}^{g}\right], \\ 0 \leq \Delta P_{\mathrm{Gd}}^{g}(t) \leq \Delta P_{\mathrm{Gdmax}}^{g}(t) \leq \min\left[(P_{G}^{g}(t) - P_{G,\mathrm{min}}^{g}), r_{d}^{g}P_{\mathrm{Gmax}}^{g}\right]. \end{cases} \tag{21}$$

(b) BESS reserve capacity constraint is as follows:

$$0 \leq V_{c}^{b}(t) + V_{d}^{b}(t) \leq V_{b,\mathrm{max}}. \tag{22}$$

(c) SOC constraint with BESS reserve capacity is as follows:

In order to ensure that the BESS can provide backup to cope with the risk of wind forecast error time t, the SOC constraint including the BESS reserve capacity is proposed as follows:

$$\begin{cases} S_{b}(t+1) = (1 - \sigma_{b})S_{b}(t) - \dfrac{1}{V_{b,\mathrm{max}}}\left(\eta_{c}^{b}P_{c}^{b}(t) - \dfrac{P_{d}^{b}(t)}{\eta_{d}^{b}}\right)\Delta t, \\ \\ S_{b,\mathrm{min}} + \dfrac{V_{d}^{b}(t)}{\eta_{d}^{b}} \leq S_{b}(t) \leq S_{b,\mathrm{max}} - \eta_{c}^{b}V_{c}^{b}(t). \end{cases} \tag{23}$$

4.3. Solution of the Two-Stage Optimization Model.

The solution process of the two-stage optimization model is to first give initial values to the variables in the first stage and then to optimize the model in the second stage. The obtained results in the second stage are returned to the model of the first stage, and the two models iterate alternately to finally obtain the result. The immune genetic algorithm [27] is used to solve the first stage problem, and the CPLEX solver in MATLAB is used to solve the second stage problem.

In this paper, the reserve capacity of BESS is optimized with the objective of minimizing the risk cost of wind power and the operation cost of thermal power units after the thermal power output and BESS charging and discharging power are determined. Therefore, this paper uses a two-stage optimization model to describe the BESS optimization problem. The convergence condition is as follows:

$$x_{i} = \sum_{t=1}^{T}\sum_{b=1}^{N_{B}}\left|V_{c,i}^{b}(t) + V_{d,i}^{b}(t) - V_{c,i-1}^{b}(t) + V_{d,i-1}^{b}(t)\right| \leq \varepsilon, \tag{24}$$

where $V_{c,i}^{b}(t)$ and $V_{d,i}^{b}(t)$ are charging and discharging reserve capacity of BESS b at iteration i, respectively, and ε is a positive number small enough. The algorithm flowchart is shown in Figure 2.

5. Results and Discussion

5.1. Simulation Setup.

IEEE30 node 6-machine systems are used to verify the model built in this paper. The system includes six coal-fired thermal power units with the same capacity of 100 MW, a wind farm with a capacity of 200 MW, and an energy storage system with the capacity of 200 MW. The maximum and minimum output power of the wind farm is 200 MW and 0, respectively. Parameters of thermal power units and BESS are given in Tables 1 and 2, and predicted data of load and wind power are given in Figure 3. According to the carbon emission intensity curves of actual coal-fired units under different load rates, the linear function between thermal power and carbon emission intensity is obtained through linear regression.

$$I_{g}\left(P_{G}^{g}(t)\right) = -120 \cdot \left(\frac{P_{G}^{g}(t)}{P_{\mathrm{Gmax}}^{g}}\right) + 1091.8. \tag{25}$$

Other parameters are as follows: wind power risk cost coefficients are $\mu_{W} = \mu_{L} = 100$. Start-stop coefficients of thermal power are $T_{g,\mathrm{on}} = T_{g,\mathrm{off}} = 4h$. BESS charge and discharge efficiency $\sigma_{b} = 0.9$, $\eta_{c}^{b} = \eta_{d}^{b} = 0.85$, initial SOC = 0.5, and $\Delta t = 1$. Carbon emission credit price is 10\$/t.

5.2. Optimization Results Analysis

5.2.1. Comparison of Different Algorithms.

The multi-objective algorithm for the two-stage model proposed in this paper is the immune genetic algorithm (IGA) [27]. In order to show the superiority of IGA in solving the model, the calculation results of IGA and of the traditional genetic algorithm (GA) were compared under the same setting of relevant parameters.

The simulation results of IGA, GA, and particle swarm optimization (PSO) are compared. The crossover probability of GA is 0.9, and the mutation probability is 0.1. The self-learning factor and social learning factor of the PSO are 2, with an initial inertia weight value of 0.9 and a maximum inertia weight value of 0.4. The other parameters of the algorithm remain unchanged, and the simulation results are shown in Table 3. The convergence curves of the algorithm are shown in Figure 4.
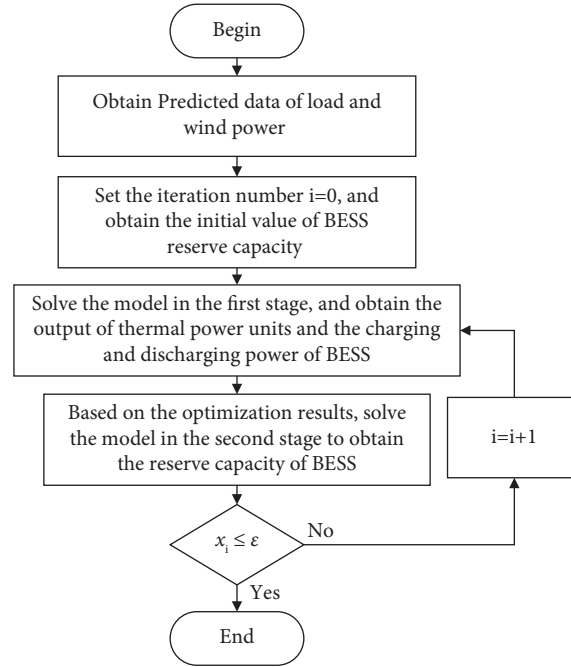
FIGURE 2: The algorithm flowchart of the two-stage operation model iteration process.

TABLE 1: Parameters of thermal power (MW).

Categories	$P_{G,\min}^g$	$P_{G\max}^g$	$r_u^g P_{G\max}^g$	$r_d^g P_{G\max}^g$
Power	0	100	20	20

TABLE 2: Parameters of BESS.

Categories	$S_{b,\max}$ (MWh)	$S_{b,\min}$ (MWh)	$P_{c\max}^b$ (MW)	$P_{d\max}^b$ (MW)
Power	180	20	100	100
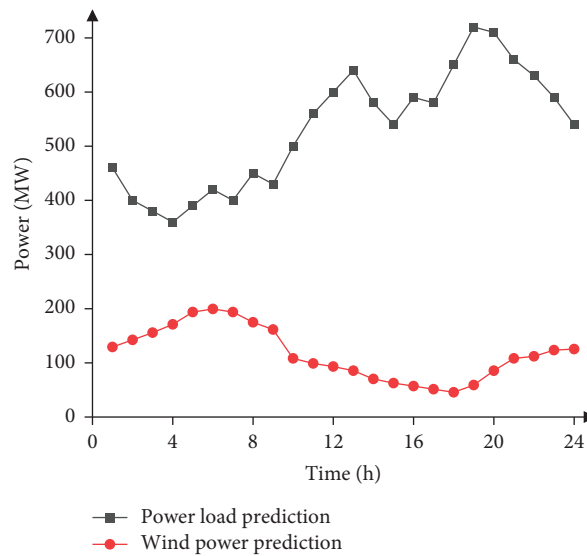
FIGURE 3: Predicted data of load and wind power.

TABLE 3: Performance comparison of different algorithms.

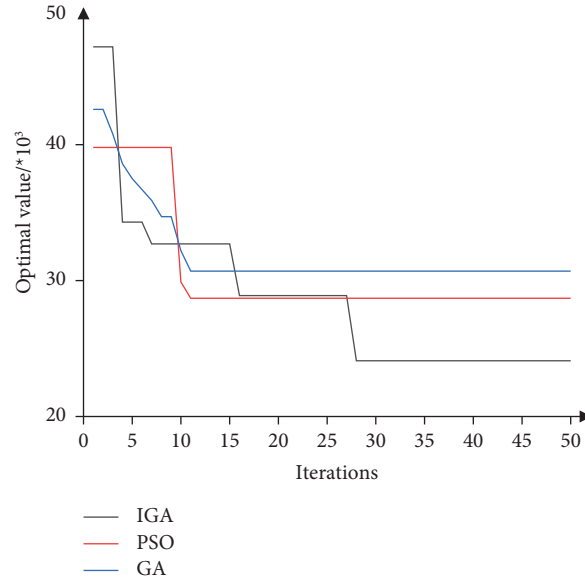| Algorithms	Optimal values ($\times 10^3$)	Time (s)
IGA	24.11	19.64
PSO	28.72	36.24
GA	30.71	20.33

FIGURE 4: Convergence curves of different algorithms.

It can be seen from the simulation results that in solving accuracy, the IGA can effectively overcome population precocity, enabling the algorithm to jump out of the local optimal solution and find a better solution. However, the IGA has limited ability to explore new spaces and is prone to convergence to the local optimal solution. Moreover, the algorithm belongs to the random algorithm, resulting in poor reliability and instability in obtaining the optimal solution. Therefore, the selection of algorithm parameters needs to refer to examples from existing references.

5.2.2. Comparison of Optimization Results. In this paper, three cases are set for comparative analysis. Under the same system settings, the optimization results are shown in Table 4. Case 1 is the model in this paper; Case 2: the BESS does not participate in the optimization of reserve capacity in the second stage; and Case 3 is that the BESS participates in the optimization of reserve capacity, but the carbon emission measurement in the first stage does not include the power of the BESS.

It can be seen from Table 4 that the system carbon emissions of cases 1 and case 2 are slightly lower than those of case 3. The difference between the carbon emissions of case 1 and case 3 is the contribution of the BESS charging and discharging power to the system's carbon emissions. The power of BESS is added to the carbon emission measurement model in case 1 to describe the real carbon emissions of the system. Different from case 3, the model proposed in this paper takes into account the contribution of the BESS, so that the BESS power needs to be as large as possible, thus

reducing the reserve capacity and increasing the risk cost of wind power and load shedding risk cost. However, the large power of BESS can reduce the operation of thermal power units, that is, reducing the operation risk and cost of thermal power units. Therefore, case 1 still has the lowest total cost.

In Table 4, the carbon emission of case 2 is lower than that of case 1. Due to the uncertainty of wind power, the BESS reserve capacity may lead to the BESS not fully utilized, resulting in reserved redundancy. In case 2, because there is no BESS reserve capacity, the power of BESS is the largest, the BESS operation cost is the highest, the peak-valley difference rate is the smallest, and the risk of load shedding and wind abandonment and operation cost of thermal power units are the largest.

Figure 5 shows the SOC curves for three cases. The optimization results of the BESS reserve capacity in case 1 and case 3 are shown in Figures 6 and 7. In cases 1 and 3, the BESS system needs to reserve a certain capacity, which leads to its conservative operation. At 1:00–7:00, the SOC of case 1 is smaller than that of case 2. This is because the wind power output is large, and case 1 reserves a certain amount of upper capacity, thus reducing the charging power in this period. During 12:00–20:00, the wind power output is small and the load power is large, so a certain lower capacity is reserved for BESS, which reduces the discharge power during this period. Case 3 is more extreme than case 2, with sufficient reserve capacity in all periods. This is because case 3 does not calculate the carbon emission benefits brought by BESS, so that BESS is almost used as a backup device.

TABLE 4: Comparison of optimization results of different cases.

	Carbon emissions (t)	BESS operation cost ($)	Peak-valley difference (%)	Load shedding risk cost ($)	Wind power risk cost ($)	Ramping cost of thermal power units ($)	Total cost ($)
Case 1	9570.7	3909	47.47	21948	26472	17721	165750
Case 2	9314.3	6755	42.45	23902	28082	22866	178990
Case 3	9974.9	6638	42.86	20784	16868	23188	167230
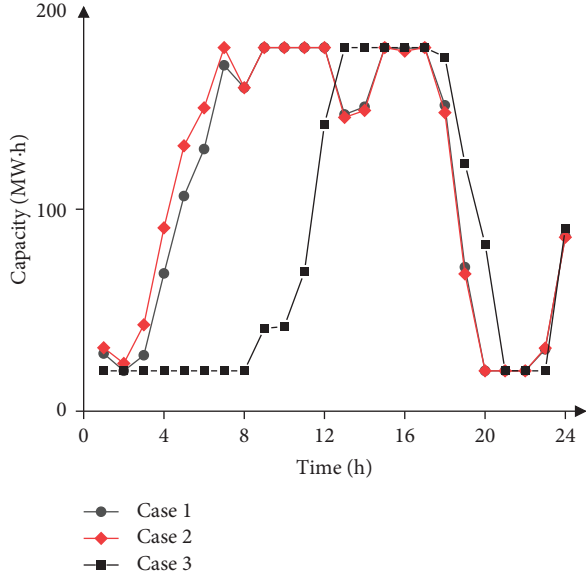
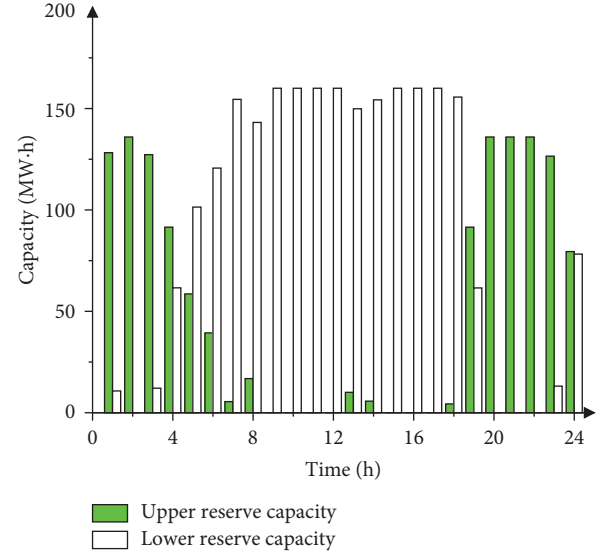FIGURE 5: The optimization results of the SOC in different cases.

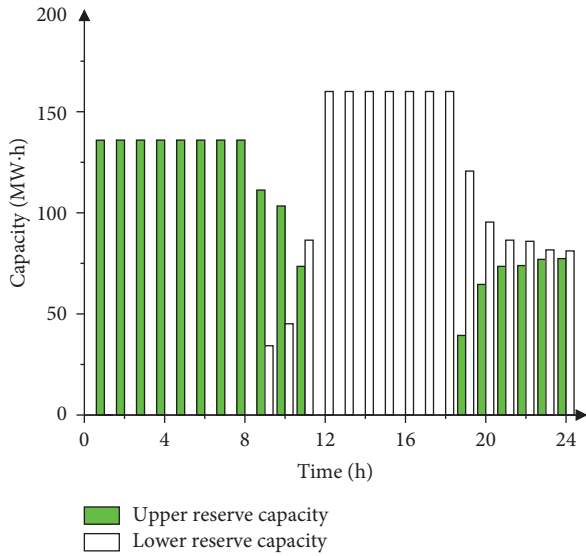FIGURE 7: Case 3: BESS optimization results at all time intervals.

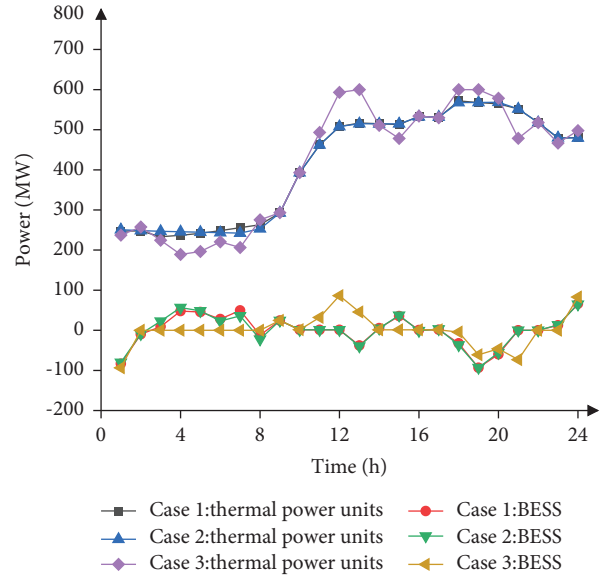FIGURE 6: Case 1: BESS optimization results at all time intervals.

FIGURE 8: The power of thermal units and BESS.

The power of thermal units and BESS in 3 cases is shown in Figure 8. Case 1 is similar to case 2. In case 2, since the BESS does not participate in the backup, the charging and discharging power of the BESS is larger at all times. In case 3, since the carbon emission benefits brought by the BESS are not calculated, the BESS is almost used as a backup, and the output of thermal power units needs to be adjusted to maintain power balance, resulting in the highest operation cost of thermal power units and the largest system carbon emissions. However, in case 3, since BESS is used as backup equipment, the risk cost of wind power is the lowest.

5.2.3. Comparison of Carbon Emission Models. In this paper, the carbon emission intensity of thermal power units is negatively related to the load, that is, the higher the load, the

lower the carbon emission intensity, as shown in Figure 9. It can be seen from Table 5 that the model with a fixed carbon emission intensity overestimates the carbon emissions of thermal power units.

In this carbon emission model, when the value of $\omega_t = r \times \min(I_g(P_G^g(t)))$ in the model increases from $0.1 \times \min(I_g(P_G^g(t)))$ to $1 \times \min(I_g(P_G^g(t)))$, the BESS charging and discharging power will be slightly increased, and the power of thermal units will be slightly reduced, which will reduce the total carbon emissions of the system. When $\omega_t > \min(I_g(P_G^g(t)))$, the model will have no solution. The case 3 in this paper is when $\omega_t = 0$.

Figures 10 and 11 show the power of the BESS and thermal units when $t = 13$ under different values of ω_t, and the BESS is in the discharge state at this time interval. With
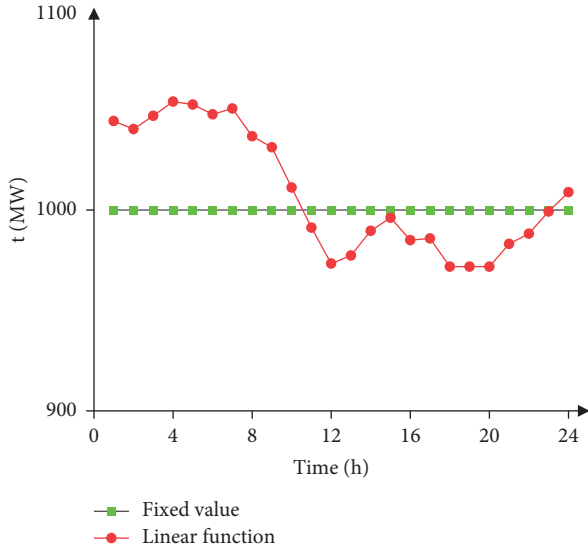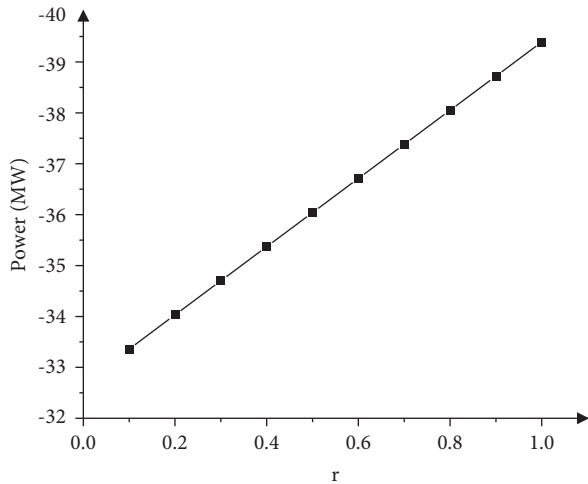
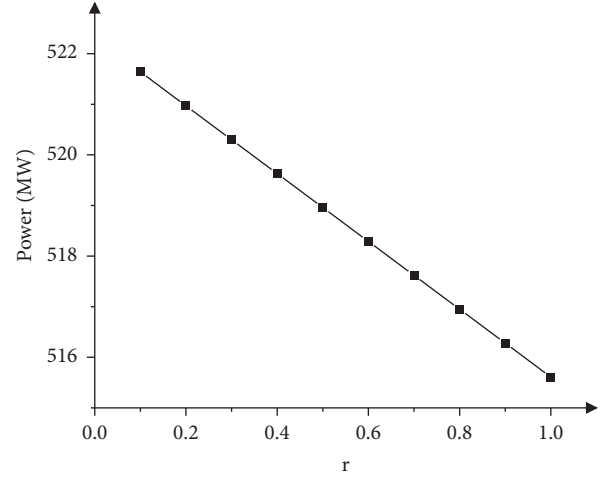FIGURE 9: Carbon emission intensity of thermal power units.

TABLE 5: Comparison of system carbon emissions.

	Carbon emissions (t)
Fixed value	9971.8
Linear function	9950.3

FIGURE 10: Variation curve of the power of BESS at different ω_t values.

the increase of the value of ω_t, the BESS discharge power increases linearly, and the power of the thermal units decreases linearly, so the increase of the BESS discharge power is equal to the decrease of the power of the thermal units. This is because the larger the value of ω_t is, the greater the carbon emission intensity of the BESS is. In order to minimize the objective function E_c, when the load is a fixed value, the BESS discharge power will increase and the power of thermal units will be reduced accordingly.

Similarly, when the BESS is charging, the greater the ω_t is, the greater the BESS charging power is, and the power of

FIGURE 11: Variation curve of the power of thermal units at different ω_t values.

thermal units will also increase accordingly. However, the increase in the power of thermal units will reduce its carbon emission intensity, so the objective function E_c can still be optimal. By increasing the value of ω_t, the carbon emission intensity of the BESS can be increased, making the BESS operation strategy more radical.

6. Conclusion

This paper includes the negative correlation between the carbon emission intensity of thermal power units and the load into the carbon emission measurement model, which improves the accuracy of carbon emission measurement of thermal power units. The system carbon emissions reduced by BESS are included in the carbon emission measurement, and it is proposed that the carbon emission intensity of BESS is related to the carbon emission intensity of thermal power units. Setting different values of ω_t can change the power of BESS and thermal units. The larger the ω_t, the greater the power of BESS, the lower the power of the thermal units, and the lower the carbon emissions of the system.

The risk cost of wind power is described by the distribution of wind forecast error, and the risk cost function of wind power with BESS reserve capacity is proposed in this paper. When the grid-side BESS has maximum reserve capacity, the risk cost of wind power can be significantly reduced, that is, the risk of load shedding and wind abandonment, and the operation cost of thermal power units can be reduced.

In the two-stage optimization model, the objective function in the first stage model is to minimize carbon emissions and load peak-valley difference by the operation of BESS, and the objective function in the second stage model is to minimize the system operation cost with the maximum reserve capacity of BESS. The first stage decision variables and the second stage decision variables restrict each other, providing an operation strategy of low carbon and flexible peak shaving for BESS.

Nomenclature

I_g:	Carbon emission intensity of thermal power units
ω_t:	Carbon emission intensity of BESS
k, b:	Linear coefficients of carbon emission intensity
μ_W:	Penalty coefficient of wind abandonment
μ_L:	Penalty coefficient of load shedding
a_g, b_g, c_g:	Fuel cost coefficients of thermal power units
d_g:	Ramping cost coefficient of thermal power units
k_1, k_2, k_3:	Weight coefficients of objective functions
$c_{B,b}$:	Operation cost coefficient of BESS
ε:	A positive number small enough
σ_b:	Self-discharge rate
η_c^b:	Charge efficiency
η_d^b:	Discharge efficiency
$V_{c,i}^b$:	Charging reserve capacity of BESS
$V_{d,i}^b$:	Discharging reserve capacity of BESS
P_G^g:	Power of thermal power units
P_c^b:	Charge power of BESS
P_d^b:	Discharge power of BESS
P_W^w:	Power of wind farm
P_K^k:	Load power on node k
ΔP_{Gu}^g:	Ramp up power of thermal power units
ΔP_{Gd}^g:	Ramp down power of thermal power units
V_c^b:	Charging reserve capacity of BESS
V_d^b:	Discharging reserve capacity of BESS
p:	Probability density function of the wind forecast error
ΔP_W^w:	Wind forecast error of wind farm
S_b:	State of charge of BESS
u_g:	Startup and shutdown status of thermal power units
ρ:	Load peak-valley ratio
N_G:	Number of thermal power units
N_B:	Number of BESS
N_W:	Number of wind farms
N_K:	Number of nodes
P_{Gg}:	Installed capacity of the thermal power units
C_B:	BESS operation cost function
E_c:	Carbon emission function of thermal power units
C_g:	Fuel cost function of thermal power units
$P_{W\max}^w$:	Maximum power of wind farm
$P_{W\min}^w$:	Minimum power of wind farm
$P_{c\max}^b$:	Maximum charge power of BESS
$P_{d\max}^b$:	Maximum discharge power of BESS
P_{W+}^w:	Upper limits of the wind forecast error
P_{W-}^w:	Lower limits of the wind forecast error
$\Delta P_{Gu\max}^g$:	Maximum ramp up limit of thermal power units
$\Delta P_{Gd\max}^g$:	Maximum ramp down limit of thermal power units
$P_{G\max}^g$:	Maximum power of thermal power units
$P_{G,\min}^g$:	Minimum power of thermal power units
$S_{b,\max}$:	Upper limits of state of charge
$S_{b,\min}$:	Lower limits of state of charge
$T_{g,\text{on}}$:	Maximum continuous start time of thermal power units
$T_{g,\text{off}}$:	Maximum continuous stop time of thermal power units
Δt:	Time between two consecutive time steps, in this paper, $\Delta t = 1$ hour
T:	Number of time intervals in one day, $T = 24$.

Data Availability

The data used to support the findings of this study are included within the article.

Conflicts of Interest

The authors declare that there are no conflicts of interest.

Acknowledgments

References

[1] Y. Meng, Y. Cao, J. Li et al., "The real cost of deep peak shaving for renewable energy accommodation in coal-fired power plants: calculation framework and case study in China," *Journal of Cleaner Production*, vol. 367, Article ID 132913, 2022.

[2] X. Jin, B. Liu, S. Liao et al., "Wasserstein metric-based two-stage distributionally robust optimization model for optimal daily peak shaving dispatch of cascade hydroplants under renewable energy uncertainties," *Energy*, vol. 260, Article ID 125107, 2022.

[3] J. Wang, S. Zhang, J. Huo, Y. Zhou, L. Li, and T. Han, "Dispatch optimization of thermal power unit flexibility transformation under the deep peak shaving demand based on invasive weed optimization," *Journal of Cleaner Production*, vol. 315, Article ID 128047, 2021.

[4] J. Liang, X. Zhao, and S. Yang, "Collaborative optimization model of renewable energy development considering peak shaving costs of various flexibility resources," *Global Energy Interconnection*, vol. 4, no. 4, pp. 394–404, 2021.

[5] A. A. Kebede, T. Kalogiannis, J. Van Mierlo, and M. Berecibar, "A comprehensive review of stationary energy storage devices for large scale renewable energy sources grid integration," *Renewable and Sustainable Energy Reviews*, vol. 159, Article ID 112213, 2022.

[6] T. M. Masaud, O. Oyebanjo, and P. K. Sen, "Sizing of large-scale battery storage for offgrid wind power plant considering a flexible wind supply-demand balance," *IET Renewable Power Generation*, vol. 11, no. 13, pp. 1625–1632, 2017.

[7] Q. Liu, R. Tian, C. Hong, and S. Pang, "Three-layer management strategy of V2G, renewable energy and energy storage based on fuzzy control," *IEEJ Transactions on Electrical and Electronic Engineering*, vol. 17, no. 9, pp. 1330–1338, 2022.

[8] T. Hou, R. Fang, D. Yang, W. Zhang, and J. Tang, "Energy storage system optimization based on a multi-time scale decomposition-coordination algorithm for wind-ESS systems," *Sustainable Energy Technologies and Assessments*, vol. 49, Article ID 101645, 2022.

[9] A. Y. Ali, A. Hussain, J.-W. Baek, and H.-M. Kim, "Optimal operation of static energy storage in fast-charging stations considering the trade-off between resilience and peak shaving," *Journal of Energy Storage*, vol. 53, Article ID 105197, 2022.

[10] A. Ebrahimi and M. Ziabasharhagh, "Introducing a novel control algorithm and scheduling procedure for optimal operation of energy storage systems," *Energy*, vol. 252, Article ID 123991, 2022.

[11] M. Ma, H. Huang, X. Song, F. Pena-Mora, Z. Zhang, and J. Chen, "Optimal sizing and operations of shared energy storage systems in distribution networks: a bi-level programming approach," *Applied Energy*, vol. 307, Article ID 118170, 2022.

[12] S.-J. Lee, J.-H. Kim, C.-H. Kim et al., "Coordinated control algorithm for distributed battery energy storage systems for mitigating voltage and frequency deviations," *IEEE Transactions on Smart Grid*, vol. 7, no. 3, pp. 1713–1722, 2016.

[13] X. Li and S. Wang, "Energy management and operational control methods for grid battery energy storage systems," *CSEE Journal of Power and Energy Systems*, vol. 7, no. 5, pp. 1026–1040, 2021.

[14] X. Li, G. Geng, Q. Jiang, J. Ma, Q. Ni, and K. Guo, "Case study of power allocation strategy for a grid-side lead-carbon battery energy storage system," *IET Renewable Power Generation*, vol. 16, no. 2, pp. 435–446, 2022.

[15] T. Gao, L. Jiang, K. Liu et al., "Field exploration and analysis of power grid side battery energy storage system," *IEEE Access*, vol. 9, pp. 63213–63218, 2021.

[16] X. Jiang, Y. Jin, X. Zheng, G. Hu, and Q. Zeng, "Optimal configuration of grid-side battery energy storage system under power marketization," *Applied Energy*, vol. 272, p. 115242, 2020.

[17] X. Dui, G. Zhu, and L. Yao, "Two-stage optimization of battery energy storage capacity to decrease wind power curtailment in grid-connected wind farms," *IEEE Transactions on Power Systems*, vol. 33, no. 3, pp. 3296–3305, 2018.

[18] M. Ghofrani, A. Arabali, M. Etezadi-Amoli, and M. S. Fadali, "A framework for optimal placement of energy storage units within a power system with high wind penetration," *IEEE Transactions on Sustainable Energy*, vol. 4, no. 2, pp. 434–442, 2013.

[19] K. Baker, G. Hug, and X. Li, "Energy storage sizing taking into account forecast uncertainties and receding horizon operation," *IEEE Transactions on Sustainable Energy*, vol. 8, no. 1, pp. 331–340, 2017.

[20] M. A. Hannan, A. Q. Al-Shetwi, R. A. Begum et al., "Impact assessment of battery energy storage systems towards achieving sustainable development goals," *Journal of Energy Storage*, vol. 42, Article ID 103040, 2021.

[21] A. T. Hoang, T. V. Nguyen, and B. T. Nguyen, "The experimental evaluation of energy efficiency and carbonic emission rates for all stable loads of larger-scale (+600 MW) coal-fired power generation units in vietnam," *Energies*, vol. 15, no. 6, p. 2185, 2022.

[22] D. Bienstock, M. Chertkov, and S. Harnett, "Chance-constrained optimal power flow: risk-aware network control under uncertainty," *SIAM Review*, vol. 56, no. 3, pp. 461–495, 2014.

[23] A. A. du Plessis, J. M. Strauss, and A. J. Rix, "Short-term solar power forecasting: investigating the ability of deep learning models to capture low-level utility-scale Photovoltaic system behaviour," *Applied Energy*, vol. 285, Article ID 116395, 2021.

[24] S. S. Silva Jr and T. M. L. Assis, "Adaptive underfrequency load shedding in systems with renewable energy sources and storage capability," *Electric Power Systems Research*, vol. 189, Article ID 106747, 2020.

[25] M. S. Nazir, A. N. Abdalla, Y. Wang et al., "Optimization configuration of energy storage capacity based on the microgrid reliable output power," *Journal of Energy Storage*, vol. 32, Article ID 101866, 2020.

[26] M. Auguadra, D. Ribo-Perez, and T. Gomez-Navarro, "Planning the deployment of energy storage systems to integrate high shares of renewables: the Spain case study," *Energy*, vol. 264, Article ID 126275, 2023.

[27] J. Yang, B. Yue, F. Feng et al., "Concrete vehicle scheduling based on immune genetic algorithm," *Mathematical Problems in Engineering*, vol. 2022, Article ID 4100049, 15 pages, 2022.